ACS OMEGA

Article

http://pubs.acs.org/journal/acsodf

Photostability of the Oleic Acid-Encapsulated Water-Soluble $Cd_xSe_yZn_{1-x}S_{1-y}$ Gradient Core−Shell Quantum Dots

Junsheng Chen,[†,‡] Bin Yang,[‡] Chuanshuai Li,[†] Kaibo Zheng,[†,§] Karel Žídek,*[,†,∥] and Tõnu Pullerits*[,†]

[†]Department of Chemical Physics and NanoLund, Chemical Center, Lund University, P.O. Box 124, 22100 Lund, Sweden

[‡]State Key Laboratory of Molecular Reaction Dynamics, Dalian Institute of Chemical Physics, Chinese Academy of Sciences, 116023 Dalian, China

[§]Gas Processing Center, College of Engineering, Qatar University, P.O. Box 2713, Doha, Qatar

[∥]Regional Centre for Special Optics and Optoelectronic Systems (TOPTEC), Institute of Plasma Physics, Academy of Sciences of the Czech Republic, Za Slovankou 1782/3, 182 00 Prague 8, Czech Republic

Supporting Information

ABSTRACT: Composite systems where quantum dots (QDs) are combined with other nanomaterials (e.g., gold nanorods) in aqueous solutions have attracted broad attention—both for their potential in applications and for studies of fundamental processes. However, high-quality QDs are typically prepared in organic solvents, and the transfer of QDs to an aqueous phase is needed to create the desired QD composites. Photostability of the transferred QDs—both the steady-state and photo-induced dynamic properties—is essential for studying the processes in the composites and for their applications. We present a detailed study of the photostability of aqueous $Cd_xSe_yZn_{1-x}S_{1-y}$ gradient core−shell QDs obtained by various approaches using linker exchange and surfactant encapsulation. Beside the steady-state photoluminescence (PL) emission stability, we also study changes in the PL decay. From the variety of the studied samples, the water-soluble QDs encapsulated by a double layer of oleic acid show superior properties, that is, stable PL emission and PL decay under continuous light or pulsed-laser light irradiation. We demonstrate that the double-layer encapsulation of QDs can be used to create QDs−metal nanoparticle composites.

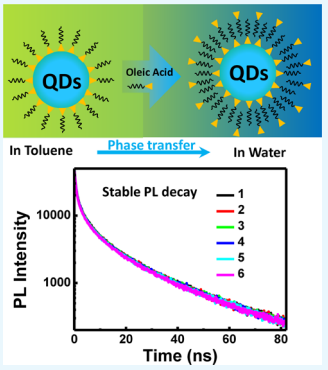

INTRODUCTION

Semiconductor nanocrystals (quantum dots, QDs) have received broad attention because of their optical properties, such as high photoluminescence (PL) quantum yield (QY), photostability, size tunability, continuous absorption band, and long luminescence lifetime.[1−4] QDs have been widely used in light-emitting diodes,[5−7] lasers,[8] photovoltaics,[9] and biomarkers.[10] Among other environments, aqueous solutions of QDs (or polar solvents in general) have been extensively studied for two main reasons: (i) combining QDs with materials natively prepared in a polar solvent (gold nanoparticles, metal-oxide nanostructures, and proteins) and (ii) use in bioapplications. Although QDs can be synthesized directly in an aqueous solution, water-based fabrication methods suffer from a wide distribution of QD sizes and a low PL QY.[11−13] On the other hand, high-quality QDs (in the sense of uniformity, size control, and crystallinity) can be readily synthesized in noncoordinating organic solvents.[11,14−16] In this case, QDs are inevitably coated with hydrophobic molecules and can be dissolved only in nonpolar media. Hence, surface modification is needed to render QDs to be water soluble.

Two strategies can be used to transfer the QDs from an organic phase to the water phase. The first strategy is the direct ligand exchange after the QDs are synthesized in an organic solvent. This is the most widely used method for phase transfer of QDs.[16−20] This process can change the chemical and physical properties of the QDs, thereby negatively influencing PL QY and dramatically decreasing the pH-sensitive stability of the QDs.[21−23] Furthermore, the exchanged ligand can be cleaved from the surface of the QDs by oxidation, and such QDs, therefore, tend to aggregate.[24] The second strategy is the surface encapsulation: QDs can be encapsulated by a silica shell layer through a surface silanization process,[25−28] coated by amphiphilic polymers[11,29−31] or a surfactant molecule layer.[11,15,17,32−34] These encapsulation methods modify the surface of QDs by adding an extra hydrophilic layer around the hydrophobic capping agent surface. Such an extra hydrophilic layer does not directly interact with QDs and therefore would not deteriorate the high stability and PL QY of QDs. This process provides significantly higher quality QDs compared with those prepared using the ligand exchange.

Most of the published studies focused on increasing the PL QY of the water-soluble QDs by the phase transfer process.[17,20,22,27,35] Nevertheless, the photostability and especially the stable photoinduced dynamic properties are important factors for aqueous QDs and their applications.

Received: March 15, 2017
Accepted: April 27, 2017
Published: May 9, 2017

DOI: 10.1021/acsomega.7b00316
ACS Omega 2017, 2, 1922−1929

Scheme 1. Schematic Diagram of the Phase Transfer QDs from Toluene to Ethanol or Water by Using Linker Exchange or Surfactant Encapsulation Strategies

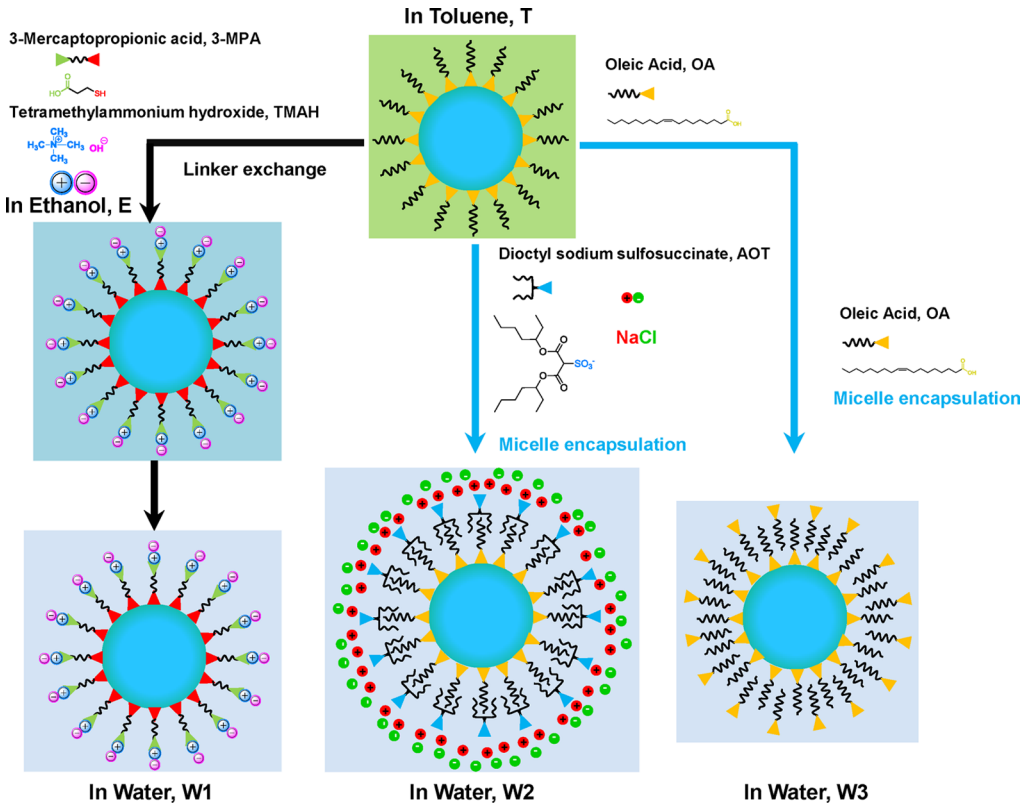

The photostability of water-soluble QDs can be affected by surface defects that are introduced during the phase transfer procedure.[24,36−38] In this article, we study water-soluble $Cd_xSe_yZn_{1-x}S_{1-y}$ gradient core−shell QDs prepared using ligand exchange and two different surfactant encapsulation methods (see Scheme 1 and Figure S1). We compare the stability of the photoinduced dynamic process of the water-soluble $Cd_xSe_yZn_{1-x}S_{1-y}$ gradient core−shell QDs by steady-state and time-resolved PL spectroscopies. We demonstrate that photostability can be used in studying the interaction between water-soluble QDs and surface plasmon (SP) objects (gold or silver nanoparticles), where the research is conditioned by PL intensity and decay stability.[39] Moreover, the results are applicable in a broad range of QD photophysics.

Our results reveal that water-soluble QDs prepared with double-layer oleic acid (OA) as a surfactant feature photostability with stable photoinduced dynamic properties. Besides this, we also demonstrate the fabrication of QDs−AuNR composite based on water-soluble QDs.

RESULTS AND DISCUSSION

We first measured the absorption and PL spectra of samples T, E, W1, W2, and W3 (see Figure 1) to verify the QD transfer to ethanol or water via linker exchanging or surfactant encapsulation. The absorption spectra of these samples overlap with each other. The PL spectra for the QDs in toluene, ethanol, and water share the same shape. We did not observe any defect emission at the red side of the band edge emission peak.[40]

In general, the PL intensity is significantly decreased after phase transfer (linker exchange and surfactant encapsulation) compared with that of the QDs before phase transfer (see

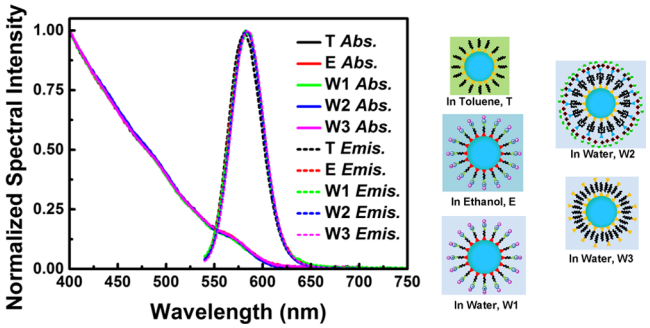

Figure 1. Normalized steady-state UV−vis absorption and PL spectra. Black solid line: absorption of QDs in toluene (T); red solid line: absorption of QDs (linker exchanged to 3-MPA) in ethanol (E); green solid line: absorption of QDs (linker exchanged to 3-MPA) in water (W1); blue solid line: absorption of QDs (AOT encapsulated) in water (W2); and pink solid line: absorption of QDs (OA encapsulated) in water (W3). Black dashed line, red dashed line, green dashed line, blue dashed line, and pink dashed line represent the PL emission spectra of T, E, W1, W2, and W3, respectively. T, E, and W1 absorption spectra cannot be distinguished.

Figure 2a), indicating the existence of PL quenching. Such a quenching can be ascribed to surface defects introduced by the phase transfer process.[36−38] However, as the surfactant encapsulation is expected to introduce less surface defects compared with the linker exchange process, the PL intensities of samples W2 and W3 are higher than those QDs obtained using the linker exchange process (samples E and W1).

To evaluate the photostability of the prepared samples, the steady-state PL intensity under continuous-wave (CW) light irradiation was measured, as shown in Figure 2b. The same

DOI: 10.1021/acsomega.7b00316
ACS Omega 2017, 2, 1922−1929

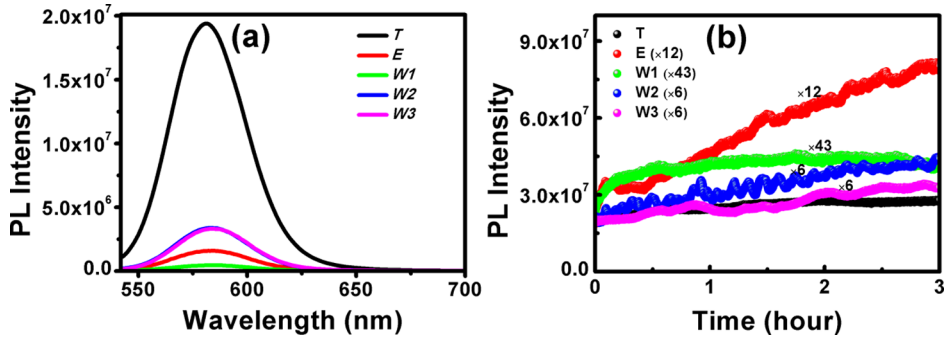

Figure 2. (a) PL spectra of T, E, W1, W2, and W3 (normalized to absorbance at excitation wavelength 450 nm, see Figure S3); (b) time-dependent PL intensity at 585 nm with a continuous light irradiation at 450 nm: black dots, red dots, green dots, blue dots, and pink dots represent the time-dependent PL intensities of T, E, W1, W2, and W3, respectively. All curves are normalized to sample T at time zero for visual convenience. The PL intensities of E, W1, W2, and W3 were multiplied by factors of 12, 43, 6, and 6, respectively.

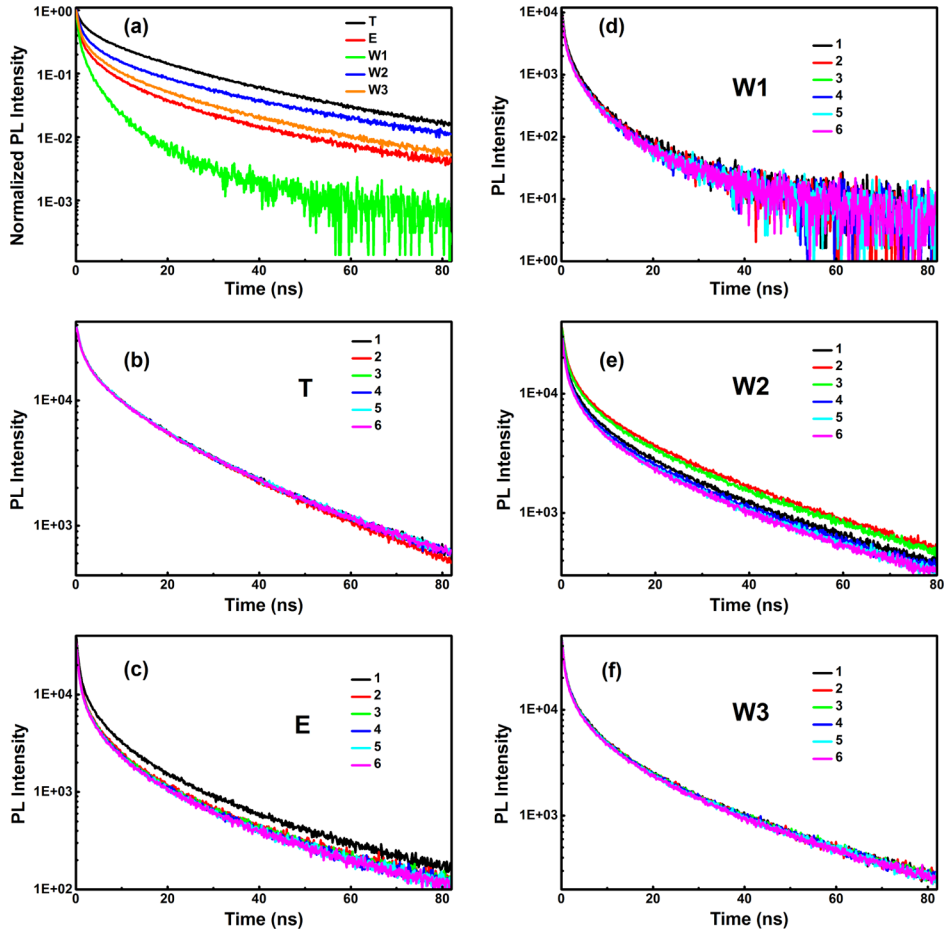

Figure 3. Stability of the photodynamic process with 438 nm picosecond-pulsed laser continuous irradiation, the PL decay was recorded at an interval of 5 min. Each decay curve took 2 min to record. (a) Normalized PL decay curve of T (black line), E (red line), W1 (green line), W2 (blue line), and W3 (orange line) at the first measurement. (b–f) illustrate the (in)stability of the PL kinetics of T, E, W1, W2, and W3, respectively. The samples were measured immediately after the preparation.

excitation power (1.3 mW/cm^2) was used here for all samples, and thus, enabling the comparison of the photostability among different samples is valid. Under 450 nm CW light irradiation, the PL intensity of all samples exhibits a general increase in the long timescale. This can be ascribed to the photoinduced surface passivation, which enhances PL emission.[24] Compared with those of samples E and W1, the PL intensity changes for samples W2 and W3 are much smaller, demonstrating a lower surface activity in the surfactant encapsulation prepared QDs. Moreover, the OA-encapsulated QDs (W3) are the most stable among all aqueous phase QDs owing to the OA double layer protecting the QD surface. After a 3 h CW light irradiation, the full width at half-maxima (FWHM) of PL emission spectra was unchanged compared with QDs before CW light irradiation (Table S1).

It should also be noted that the minor fluctuations in the PL intensity evolution in Figure 2 can be assigned to the fluctuations in the QD concentration within the irradiated

DOI: 10.1021/acsomega.7b00316
ACS Omega 2017, 2, 1922−1929

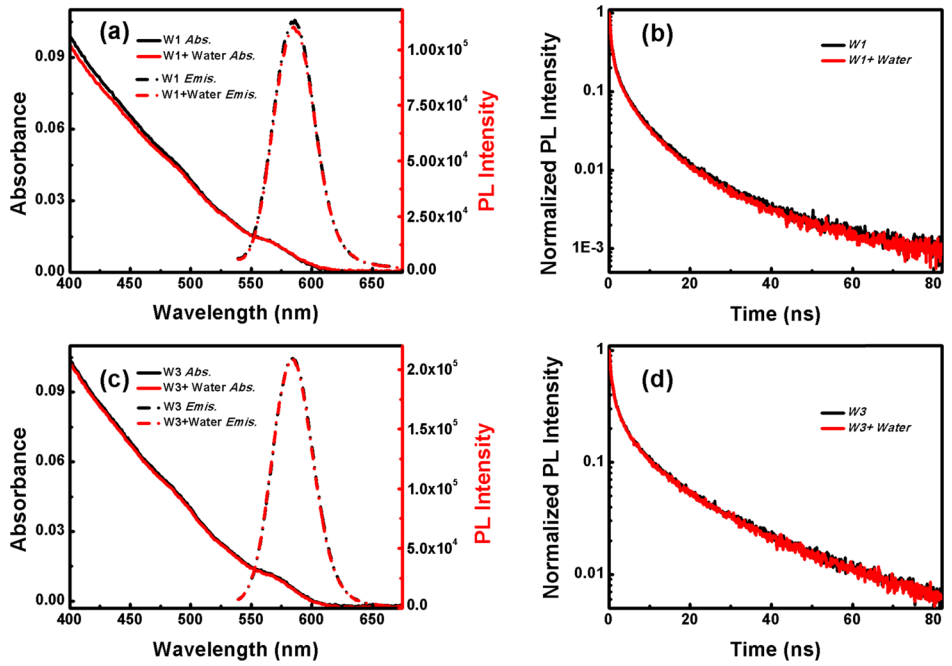

Figure 4. Absorption, PL emission, and PL decay spectra of W1, W1 with 40 μL of MQ water added, W3, and W3 with 40 μL of MQ water added. (a) Steady-state absorption and PL spectra of W1 and W1 with 40 μL of MQ water added; (b) PL decay of W1 and W1 with 40 μL of MQ water added; (c) steady-state absorption and PL spectra of W3 and W3 with 40 μL of MQ water added; and (d) PL decay of W3 and W3 with 40 μL of MQ water added.

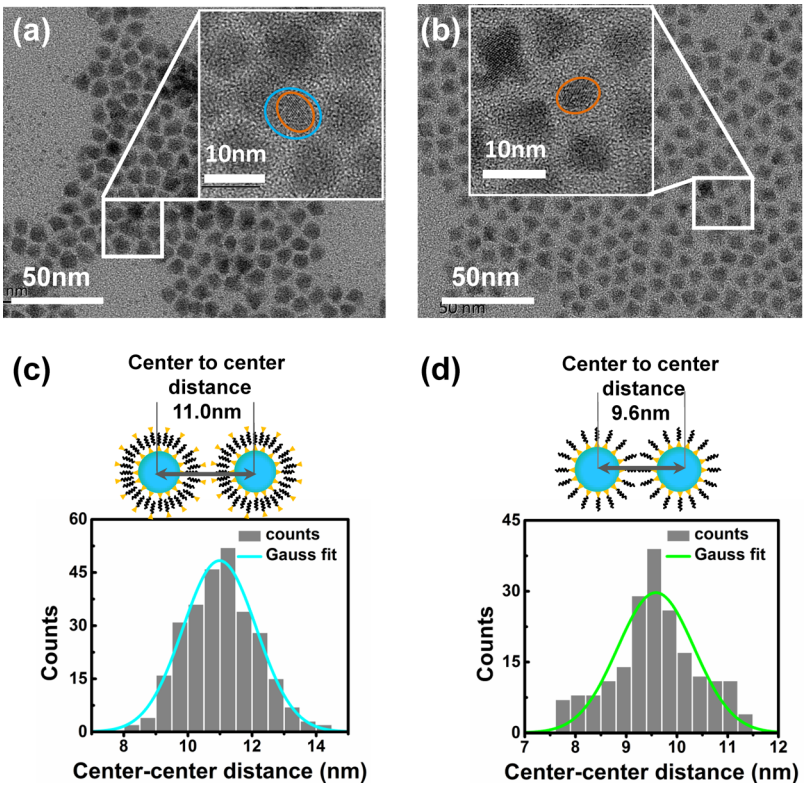

Figure 5. TEM micrographs of double-layer OA-encapsulated QDs in water (a) and QDs in toluene (b); inset: high-resolution TEM image of QDs in W3 and T, the center-to-center distance distribution histograms of two adjacent QDs in W3 (c) and in T (d).

spot or competition among processes such as H_2O adsorption, photo-oxidation, and photocorrosion on the surface of the QDs.[24]

Besides steady-state emission, the stable photoinduced dynamic properties would be another important factor to investigate the interaction between QDs and other objects (molecules, SP structures, metal-oxides, and so on). We, therefore, investigated the time evolution of PL decays of water-soluble QDs during the time-correlated single-photon-counting (TCSPC) measurement—see Figure 3. To achieve

DOI: 10.1021/acsomega.7b00316
ACS Omega 2017, 2, 1922−1929

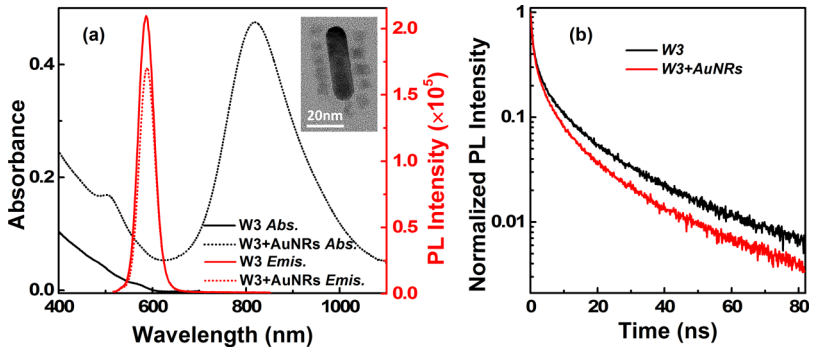

Figure 6. Absorption, PL emission, and PL decay spectra of W3 and W3 with 40 μL of AuNR water added. (a) Absorption and PL spectra of W3 and W3 with 40 μL of AuNRs added; inset: TEM micrographs of an AuNR−QD nanocomposite; (b) PL decays of W3 and W3 with 40 μL of AuNRs added.

that, we measured several sequential PL decay curves for each sample. Changes in the decay curves are a sensitive probe for photodamage.

Figure 3a summarizes the normalized very first PL decay curves for all fresh samples. W1 exhibits the fastest PL decay among these samples, which is in agreement with the lowest PL emission intensity (Figure 2a). In addition, the PL decay rate for other samples decreases progressively (T, W2, W3, E, and W1) in accordance with the trend of PL intensities in steady-state emission measurement.

Under 438 nm picosecond-pulsed laser irradiation, the consequently measured PL decays are changing over time for E and W2. The PL decay becomes faster under 438 nm laser continuous irradiation in E. For W2, the PL decay slows down for the three initial measurements, and then, it speeds up for the last two measurements. For W1, W3, and T, the TCSPC-measured decays remain stable within the six measured scans. As one can notice, sample T is the most stable one because of the as-prepared QDs with less surface defects. This indicates that surface defects can affect the photoinduced dynamic properties of QDs.

Considering the photostability results taken from both steady-state and time-resolved PL measurements, the photostability of W3 is comparable with that of the as-prepared sample in an organic solvent (T), and sample W3 is the most suitable one for studying the QDs and their composites in aqueous solution. Nevertheless, to fabricate such composites, the aqueous QDs have to remain stable with the addition of other objects or solvent; especially, the QDs have to show resistance against pH fluctuations, which can be introduced by adding a small amount of water. In our case, we verify the pH resistance by adding 40 μL of Milli-Q (MQ) water into two water-soluble QDs W3 and W1 and comparing the absorption, PL emission, and PL decay spectra (see Figure 4).

After adding 40 μL of MQ water into 3 mL of W1 solution, the absorption and PL emission intensity are decreased (see Figure 4a), whereas the PL decay becomes faster (see Figure 4b). These changes are due to the aggregation of QDs in W1, which is induced by the pH change in the solution. During the linker exchanging process, TMAH solution needs to be added to modify the surface of the negatively charged QDs. The negatively charged QDs show repulsive force against each other, thus preventing the aggregation of the QDs.[41] The electrostatic repulsion among QDs was diminished after a small amount ($V_{\mathrm{MQ\ water}}/V_{\mathrm{W1}}$ = 1.3%) of MQ water was added to W1, leading to the aggregation of QDs.

At the same time, there is no difference between W3 and W3 with 40 μL of MQ water added. We obtained identical absorption, PL emission, and PL decay spectra (see Figure 4c,d). In W3, the QDs are encapsulated in two layers of OA molecules, and a small amount ($V_{\mathrm{MQ\ water}}/V_{\mathrm{W1}}$ = 1.3%) of MQ water is not able to change the encapsulation structure. We repeated the experiments three times without observing any difference (see Figures S4 and S5).

To obtain further insight into the structure of OA-encapsulated QDs (W3), the TEM images were recorded (Figure 5). After the phase transfer, the QDs in W3 remain separated from each other without aggregation. The interparticle distance is influenced by the capping agent, and it is possible to confirm the formation of OA double layer by measuring the interparticle distance. However, one can notice that in the high-resolution TEM image not only does the crystalline structure (QDs) give the contrast (the orange circle in Figure 5 inset) but an additional thin noncrystalline layer is also clearly visible in W3 (see the blue circle in Figure 5a inset). This layer may be an amorphous capping agent or other supernatants. For the sample T, no such thin layer could be identified outside of the QDs. The extra layer in W3 cannot be ascribed to the different size of QDs because W3 and T QDs had the same size—see the nearly identical absorption spectra in Figure 1. The extra layer makes it difficult to judge the interparticle distance. Hence, we measured the center-to-center distance to confirm the formation of OA encapsulation in W3. Between two individual QDs, the center-to-center distance in W3 (11.0 ± 2.7 nm) is larger than that in T (9.6 ± 1.8 nm). The larger distance in W3 is in good agreement with the presence of double layers of OA encapsulating the QDs. The length of the OA molecule is 2 nm.[42]

The OA-encapsulated QDs show a stable photoinduced dynamic process and the encapsulation structure shows resistance for small amounts of water. Therefore, it is possible to study the interaction between W3 and other objects in the nanocomposite structures, especially the excited-state dynamic processes. A good example is the QDs−AuNR composites, which have been widely studied for plasmon interactions. Here, we combine our QDs (W3) with AuNRs in water and monitor the excited-state dynamics of such a system to obtain insights into the interaction between two parts. Figure 6 shows the absorption, PL emission, and PL decay spectra of W3 with the addition of 40 μL of AuNRs (5.1 μmol/L). The absorption spectrum of AuNRs is dominated by plasmon modes with a high extinction coefficient compared with QDs. The steady-state PL intensity of QDs is quenched, and the PL decays faster

DOI: 10.1021/acsomega.7b00316
ACS Omega 2017, 2, 1922−1929

with the addition of AuNRs (Figure 6b). The observed PL quenching can be attributed to a combination of different factors such as the large extinction coefficient of AuNRs, defects introduced by AuNRs, charge transfer,[43] and energy transfer. We can neglect the effect of AuNR reabsorption because of a moderate absorbance (OD ≈ 0.1, Figure 6a) at the PL emission peak. The defect formation is unlikely due to the passivation of the QDs via an OA double layer. At the same time, the energy transfer was reported to dominate the PL quenching for QD−metal nanoparticle donor−acceptor distance in the range of 2−6 nm.[44−46] Our QDs−AuNR nanocomposites fulfill such a condition with an OA double layer spacer. We conclude that the energy transfer is the most plausible explanation for the observed changes.

CONCLUSIONS

The photostability of water-soluble $Cd_xSe_yZn_{1-x}S_{1-y}$ gradient core−shell QDs encapsulated via three different strategies was evaluated and compared with the properties of the original QDs in toluene and QDs transferred to ethanol. The shapes of the steady-state absorption and PL emission spectra remain the same for all samples, proving that OA-capped QDs can be successfully transferred from a nonpolar solvent (toluene) to a polar solvent (ethanol or water) via both linker exchange and surfactant encapsulation methods. Nevertheless, within the studied samples, the QDs encapsulated by a double layer of OA (sample W3) feature superior stability both of the steady-state PL intensity and of nanosecond PL decay. We demonstrate that such QDs can be combined with AuNRs and form composites where energy transfer between QDs and AuNRs can be observed and studied. QDs encapsulated by a double layer of OA can be useful for developing QDs−AuNR nanocomposites and study interaction between QDs and other objects in an aqueous environment.

EXPERIMENTAL SECTION

OA (Sigma-Aldrich, 90%)-capped $Cd_xSe_yZn_{1-x}S_{1-y}$ gradient core−shell QDs were prepared by a previously reported single-step hot injection method.[16,47] A mixture of 0.4 mmol cadmium oxide (CdO, Sigma-Aldrich, 99.99%), 4 mmol zinc acetate (Sigma-Aldrich, 99.9%), and 17.6 mmol OA in 20 mL of 1-octadecene (ODE, Sigma-Aldrich, 90%) was heated to 150 °C and degassed under vacuum for 30 min. Then, the mixture was further heated up to 310 °C under a N_2 atmosphere to form a clear solution of $Cd(OA)_2$ (Cd-oleate) and $Zn(OA)_2$ (Zn-oleate), as precursors for cations. Then, a mixture of 0.4 mmol selenium powder (Se, Sigma-Aldrich, 99.9%), 4 mmol sulfur (S, Sigma-Aldrich, 99.9%), and trioctylphosphine (TOP, Sigma-Aldrich, 90%) was injected swiftly into the precursor solution. To control the shell thickness of the gradient core−shell QDs, the reaction was stopped by cooling the solution in an ice bath 3 min after the injection. To purify the as-prepared core−shell QDs, a mixture of chloroform and acetone ($V_{chloroform}/V_{acetone}$ = 1:5) was added dropwise and the QDs were centrifuged at 6500 rpm for 10 min. The purification procedure was repeated twice, and the purified OA-capped gradient core−shell QDs with an approximately 3 nm core and 1.3 nm shell[48] were then dissolved in the nonpolar organic solvent toluene (T, see Scheme 1) with a concentration of approximately 1.7 mM. The concentration was estimated based on the absorption spectrum and the extinction coefficient of the QDs, which follows a size-dependent empirical function.[49]

Ligand exchange and surfactant encapsulation methods (see Scheme 1) were used in phase transfer experiments. The ligand exchange was conducted by using the strong affiliation ability between 3-mercaptopropionic acid (3-MPA) and QDs. Four hundred microliters of stock QDs in toluene solution was mixed with 80 μL of 3-MPA and 200 μL of ethanol. The mixture was stirred for 30 min, and QDs were capped with 3-MPA and aggregated in the mixture. The aggregated QDs were collected by centrifuging the mixture for 5 min at 3500 rpm speed. The solvent was discarded, and the residual was dissolved in 40 mL of water or ethanol. Then, 75 μL of tetramethylammonium hydroxide (TMAH, Sigma-Aldrich, 25 wt %) in methanol was dropwise added to the water or ethanol QD solution, causing a clear solution with a pH value of approximately 10.[50] Finally, 3-MPA-capped QDs can be dissolved in water (W1, see Scheme 1) or ethanol (E, see Scheme 1). For the surfactant encapsulation strategy, two different surfactants were used. One was AOT (sodium bis(2-ethylhexyl)-sulfosuccinate, from Sigma-Aldrich, ≥97%), and the other one was OA.

QDs encapsulated by the AOT surfactant (W2, see Scheme 1) were prepared by a previously reported method.[34] In brief, a toluene solvent of 400 μL of QD stock solution was evaporated under vacuum at room temperature and dark condition. The remaining QD solids were then dispersed in 4 mL of hexane with the addition of 120 mg of AOT. Subsequently, the mixture was added to 40 mL of 3 g/L NaCl water solution under vigorous stirring, in which an oil-in-water (O/W) emulsion was formed. This hexane in mixture was then removed by bathing in 80 °C water with stirring for 30 min. The residual was cooled down to room temperature followed by centrifuging at 6500 rpm for 15 min. The final QD aqueous solution was collected by filtration through a syringe filter (pore size of 200 nm, VWR International), which can filter out QDs aggregates. During the experiment, no retention was observed on the filter.

OA can also be used as a surfactant for the water-soluble QD preparation.[15] Here, 80 μL of OA was added to 4 mL of the same QD suspension in hexane mentioned above. The solvent was then sonicated for 1 min. Afterward, 40 mL of MQ water (Millipore, 18.2 MΩ cm) was added to this hexane solution under vigorous stirring. Another 1 h sonication was then performed until a cloudy and colorless solution was formed. Phase separation took place after keeping this mixture undisturbed in dark for 24 h. QDs appeared at the bottom of the water phase were collected and purified by centrifuging at 6500 rpm for 15 min. Consequently, the upper clear solution would contain only QDs encapsulated by an OA double layer (W3, see Scheme 1), which can be well-dispersed in water. Such a solution would undergo final filtration through a syringe filter (pore size of 200 nm, VWR International) before usage. During the experiment, no retention was observed on the filter. The ligand exchange and the surfactant encapsulation mechanisms are shown in Scheme 1. The mechanisms are supported by Fourier transform infrared spectroscopy (FTIR) data (see Figure S1).

Water-dispersed gold nanorods (41 × 10 nm in dimension, with 6-amino-1-hexanethiol hydrochloride as conjugation) were purchased from Nanopartz.

UV−vis absorption spectra were recorded using a PerkinElmer Lambda 1050 spectrophotometer. FTIR spectra were recorded using a Nicolet iS5 FT-IR instrument. The steady-state fluorescence spectra were recorded using a Horiba Jobin Yvon Fluorolog-3 spectrofluorometer. This spectrofluor-

DOI: 10.1021/acsomega.7b00316
ACS Omega 2017, 2, 1922−1929

ometer has been used to determine the photostability of QDs. QD samples were irradiated at 450 nm by CW light with an excitation intensity of 1.3 mW/cm^2. The spot size was approximately 1 cm × 0.8 cm. The PL intensity at 585 nm was measured up to 3 h. Time-resolved PL measurements were taken using a TCSPC device (PicoQuant). A pulsed diode laser, triggered externally at 2.5 MHz, was used to excite the sample at 438 nm, with an excitation fluence of 3.3 × 10^{11} photons/cm^2/pulse. The pulse duration of the laser was approximately 200 ps. The emitted photons were focused onto a fast avalanche photodiode (SPAD, Micro Photon Device). The response time of the photodiode was <50 ps. TEM images were recorded using a JEOL JEM-2100F instrument.

■ ASSOCIATED CONTENT

Supporting Information

The Supporting Information is available free of charge on the ACS Publications website at DOI: 10.1021/acsomega.7b00316.

FTIR spectra, normalized steady-state PL spectra before and after 3 h of 450 nm continuous light irradiation; steady-state UV−vis absorption; and the absorption, PL emission, and PL decay spectra of W1 (W3) with and without 40 μL MQ water added (PDF)

■ AUTHOR INFORMATION

Corresponding Authors

*E-mail: zidek@ipp.cas.cz (K.Ž.).
*E-mail: tonu.pullerits@chemphys.lu.se (T.P.).

ORCID

Junsheng Chen: 0000-0002-2934-8030

Notes

The authors declare no competing financial interest.

■ ACKNOWLEDGMENTS

This work was financed by the Swedish Research Council (VR), the Knut and Alice Wallenberg Foundation, Interreg Öresund-Kattegat-Skagerrak, European Regional Development Fund and NPRP grant # NPRP7-227-1-034 from the Qatar National Research Fund.

■ REFERENCES

(1) Wu, P.; Yan, X.-P. Doped quantum dots for chemo/biosensing and bioimaging. *Chem. Soc. Rev.* **2013**, *42*, 5489−5521.
(2) Shamirian, A.; Ghai, A.; Snee, P. QD-Based FRET Probes at a Glance. *Sensors* **2015**, *15*, 13028−13051.
(3) Kamat, P. V. Quantum Dot Solar Cells. Semiconductor Nanocrystals as Light Harvesters. *J. Phys. Chem. C* **2008**, *112*, 18737−18753.
(4) Chen, J.; Liu, D.; Al-Marri, M. J.; Nuuttila, L.; Lehtivuori, H.; Zheng, K. Photo-stability of CsPbBr3 perovskite quantum dots for optoelectronic application. *Sci. China Mater.* **2016**, *59*, 719−727.
(5) Zheng, K.; Karki, K.; Žídek, K.; Pullerits, T. Ultrafast photoinduced dynamics in quantum dot-based systems for light harvesting. *Nano Res.* **2015**, *8*, 2125−2142.
(6) Grim, J. Q.; Manna, L.; Moreels, I. A sustainable future for photonic colloidal nanocrystals. *Chem. Soc. Rev.* **2015**, *44*, 5897−5914.
(7) Colvin, V. L.; Schlamp, M. C.; Alivisatos, A. P. Light-Emitting Diodes Made from Cadmium Selenide Nanocrystals and a Semiconducting Polymer. *Nature* **1994**, *370*, 354−357.
(8) Klimov, V. I.; Mikhailovsky, A. A.; Xu, S.; Malko, A.; Hollingsworth, J. A.; Leatherdale, C. A.; Eisler, H.-J.; Bawendi, M. G. Optical gain and stimulated emission in nanocrystal quantum dots. *Science* **2000**, *290*, 314−317.
(9) Kamat, P. V. Quantum Dot Solar Cells. The Next Big Thing in Photovoltaics. *J. Phys. Chem. Lett.* **2013**, *4*, 908−918.
(10) Bruchez, M.; Moronne, M.; Gin, P.; Weiss, S.; Alivisatos, A. P. Semiconductor nanocrystals as fluorescent biological labels. *Science* **1998**, *281*, 2013−2016.
(11) Yu, W. W.; Chang, E.; Drezek, R.; Colvin, V. L. Water-soluble quantum dots for biomedical applications. *Biochem. Biophys. Res. Commun.* **2006**, *348*, 781−786.
(12) Zhuang, J.; Zhang, X.; Wang, G.; Li, D.; Yang, W.; Li, T. Synthesis of water-soluble ZnS : Mn^{2+} nanocrystals by using mercaptopropionic acid as stabilizer. *J. Mater. Chem.* **2003**, *13*, 1853−1857.
(13) Zhan, H.; Zhou, P.; Pan, K.; He, T.; He, X.; Zhou, C.; He, Y. One-pot aqueous-phase synthesis of ultra-small CdSe/CdS/CdZnS core−shell−shell quantum dots with high-luminescent efficiency and good stability. *J. Nanopart. Res.* **2013**, *15*, 1680.
(14) Liu, L.; Guo, X.; Li, Y.; Zhong, X. Bifunctional Multidentate Ligand Modified Highly Stable Water-Soluble Quantum Dots. *Inorg. Chem.* **2010**, *49*, 3768−3775.
(15) Prakash, A.; Zhu, H.; Jones, C. J.; Benoit, D. N.; Ellsworth, A. Z.; Bryant, E. L.; Colvin, V. L. Bilayers as Phase Transfer Agents for Nanocrystals Prepared in Nonpolar Solvents. *ACS Nano* **2009**, *3*, 2139−2146.
(16) Bae, W. K.; Char, K.; Hur, H.; Lee, S. Single-step synthesis of quantum dots with chemical composition gradients. *Chem. Mater.* **2008**, *20*, 531−539.
(17) Zhang, Y.; Clapp, A. Overview of Stabilizing Ligands for Biocompatible Quantum Dot Nanocrystals. *Sensors* **2011**, *11*, 11036−11055.
(18) Skaff, H.; Emrick, T. The use of 4-substituted pyridines to afford amphiphilic, pegylated cadmium selenide nanoparticles. *Chem. Commun.* **2003**, 52−53.
(19) Locklin, J.; Patton, D.; Deng, S.; Baba, A.; Millan, M.; Advincula, R. C. Conjugated oligothiophene-dendron-capped CdSe nanoparticles: Synthesis and energy transfer. *Chem. Mater.* **2004**, *16*, 5187−5193.
(20) Liu, Y.; Kim, M.; Wang, Y.; Wang, Y. A.; Peng, X. Highly luminescent, stable, and water-soluble CdSe/CdS core−shell dendron nanocrystals with carboxylate anchoring groups. *Langmuir* **2006**, *22*, 6341−6345.
(21) Debruyne, D.; Deschaume, O.; Coutiño-Gonzalez, E.; Locquet, J.-P.; Hofkens, J.; Van Bael, M. J.; Bartic, C. The pH-dependent photoluminescence of colloidal CdSe/ZnS quantum dots with different organic coatings. *Nanotechnology* **2015**, *26*, 255703.
(22) Gao, M.; Kirstein, S.; Möhwald, H.; Rogach, A. L.; Kornowski, A.; Eychmüller, A.; Weller, H. Strongly photoluminescent CdTe nanocrystals by proper surface modification. *J. Phys. Chem. B* **1998**, *102*, 8360−8363.
(23) Zhang, H.; Zhou, Z.; Yang, B.; Gao, M. The influence of carboxyl groups on the photoluminescence of mercaptocarboxylic acid-stabilized CdTe nanoparticles. *J. Phys. Chem. B* **2003**, *107*, 8−13.
(24) Carrillo-Carrión, C.; Cárdenas, S.; Simonet, B. M.; Valcárcel, M. Quantum dots luminescence enhancement due to illumination with UV/Vis light. *Chem. Commun.* **2009**, 5214−5226.
(25) Darbandi, M.; Thomann, R.; Nann, T. Single quantum dots in silica spheres by microemulsion synthesis. *Chem. Mater.* **2005**, *17*, 5720−5725.
(26) Stöber, W.; Fink, A.; Bohn, E. Controlled Growth of Monodisperse Silica Spheres in the Micron Size Range. *J. Colloid Interface Sci.* **1968**, *26*, 62−69.
(27) Qian, L.; Bera, D.; Tseng, T.-K.; Holloway, P. H. High efficiency photoluminescence from silica-coated CdSe quantum dots. *Appl. Phys. Lett.* **2009**, *94*, 073112.
(28) Hu, X.; Zrazhevskiy, P.; Gao, X. Encapsulation of Single Quantum Dots with Mesoporous Silica. *Ann. Biomed. Eng.* **2009**, *37*, 1960−1966.
(29) Yu, W. W.; Chang, E.; Falkner, J. C.; Zhang, J.; Al-Somali, A. M.; Sayes, C. M.; Johns, J.; Drezek, R.; Colvin, V. L. Forming

DOI: 10.1021/acsomega.7b00316
ACS Omega 2017, 2, 1922−1929

biocompatible and nonaggregated nanocrystals in water using amphiphilic polymers. *J. Am. Chem. Soc.* **2007**, *129*, 2871−2879.
(30) Pellegrino, T.; Manna, L.; Kudera, S.; Liedl, T.; Koktysh, D.; Rogach, A. L.; Keller, S.; Rädler, J.; Natile, G.; Parak, W. J. Hydrophobic nanocrystals coated with an amphiphilic polymer shell: A general route to water soluble nanocrystals. *Nano Lett.* **2004**, *4*, 703−707.
(31) Anderson, R. E.; Chan, W. C. W. Systematic investigation of preparing biocompatible, single, and small ZnS-capped CdSe quantum dots with amphiphilic polymers. *ACS Nano* **2008**, *2*, 1341−1352.
(32) Wang, J.; Han, S.; Ke, D.; Wang, R. Semiconductor Quantum Dots Surface Modification for Potential Cancer Diagnostic and Therapeutic Applications. *J. Nanomater.* **2012**, *2012*, 1−8.
(33) Wang, Y.; Wong, J. F.; Teng, X.; Lin, X. Z.; Yang, H. "Pulling" nanoparticles into water: Phase transfer of oleic acid stabilized monodisperse nanoparticles into aqueous solutions of α-cyclodextrin. *Nano Lett.* **2003**, *3*, 1555−1559.
(34) Bagaria, H. G.; Kini, G. C.; Wong, M. S. Electrolyte Solutions Improve Nanoparticle Transfer from Oil to Water. *J. Phys. Chem. C* **2010**, *114*, 19901−19907.
(35) Wang, M.; Felorzabihi, N.; Guerin, G.; Haley, J. C.; Scholes, G. D.; Winnik, M. A. Water-soluble CdSe quantum dots passivated by a multidentate diblock copolymer. *Macromolecules* **2007**, *40*, 6377−6384.
(36) Dubois, F.; Mahler, B.; Dubertret, B.; Doris, E.; Mioskowski, C. A versatile strategy for quantum dot ligand exchange. *J. Am. Chem. Soc.* **2007**, *129*, 482−483.
(37) Wang, Q.; Xu, Y.; Zhao, X.; Chang, Y.; Liu, Y.; Jiang, L.; Sharma, J.; Seo, D.-K.; Yan, H. A facile one-step in situ functionalization of quantum dots with preserved photoluminescence for bioconjugation. *J. Am. Chem. Soc.* **2007**, *129*, 6380−6381.
(38) Zillner, E.; Fengler, S.; Niyamakom, P.; Rauscher, F.; Köhler, K.; Dittrich, T. Role of Ligand Exchange at CdSe Quantum Dot Layers for Charge Separation. *J. Phys. Chem. C* **2012**, *116*, 16747−16754.
(39) Chen, J.; Žídek, K.; Abdellah, M.; Al-Marri, M. J.; Zheng, K.; Pullerits, T. Surface plasmon inhibited photo-luminescence activation in CdSe/ZnS core−shell quantum dots. *J. Phys.: Condens. Matter* **2016**, *28*, 254001.
(40) Abdellah, M.; Karki, K. J.; Lenngren, N.; Zheng, K.; Pascher, T.; Yartsev, A.; Pullerits, T. Ultra Long-Lived Radiative Trap States in CdSe Quantum Dots. *J. Phys. Chem. C* **2014**, *118*, 21682−21686.
(41) Qu, F.; Morais, P. C. The pH dependence of the surface charge density in oxide-based semiconductor nanoparticles immersed in aqueous solution. *IEEE Trans. Magn.* **2001**, *37*, 2654−2656.
(42) Theis-Bröhl, K.; Gutfreund, P.; Vorobiev, A.; Wolff, M.; Toperverg, B. P.; Dura, J. A.; Borchers, J. A. Self assembly of magnetic nanoparticles at silicon surfaces. *Soft Matter* **2015**, *11*, 4695−4704.
(43) Adams, D. M.; Brus, L.; Chidsey, C. E. D.; Creager, S.; Creutz, C.; Kagan, C. R.; Kamat, P. V.; Lieberman, M.; Lindsay, S.; Marcus, R. A.; Metzger, R. M.; Michel-Beyerle, M. E.; Miller, J. R.; Newton, M. D.; Rolison, D. R.; Sankey, O.; Schanze, K. S.; Yardley, J.; Zhu, X. Charge transfer on the nanoscale: Current status. *J. Phys. Chem. B* **2003**, *107*, 6668−6697.
(44) Focsan, M.; Gabudean, A. M.; Vulpoi, A.; Astilean, S. Controlling the Luminescence of Carboxyl-Functionalized CdSe/ZnS Core−Shell Quantum Dots in Solution by Binding with Gold Nanorods. *J. Phys. Chem. C* **2014**, *118*, 25190−25199.
(45) Li, M.; Cushing, S. K.; Wang, Q.; Shi, X.; Hornak, L. A.; Hong, Z.; Wu, N. Size-Dependent Energy Transfer between CdSe/ZnS Quantum Dots and Gold Nanoparticles. *J. Phys. Chem. Lett.* **2011**, *2*, 2125−2129.
(46) Kim, D.; Yokota, H.; Taniguchi, T.; Nakayama, M. Precise control of photoluminescence enhancement and quenching of semiconductor quantum dots using localized surface plasmons in metal nanoparticles. *J. Appl. Phys.* **2013**, *114*, 154307.
(47) Žídek, K.; Zheng, K.; Abdellah, M.; Lenngren, N.; Chábera, P.; Pullerits, T. Ultrafast Dynamics of Multiple Exciton Harvesting in the CdSe−ZnO System: Electron Injection versus Auger Recombination. *Nano Lett.* **2012**, *12*, 6393−6399.
(48) Abdellah, M.; Žídek, K.; Zheng, K.; Chábera, P.; Messing, M. E.; Pullerits, T. Balancing Electron Transfer and Surface Passivation in Gradient CdSe/ZnS Core−Shell Quantum Dots Attached to ZnO. *J. Phys. Chem. Lett.* **2013**, *4*, 1760−1765.
(49) Yu, W. W.; Qu, L.; Guo, W.; Peng, X. Experimental determination of the extinction coefficient of CdTe, CdSe, and CdS nanocrystals. *Chem. Mater.* **2003**, *15*, 2854−2860.
(50) Zheng, K.; Žídek, K.; Abdellah, M.; Torbjörnsson, M.; Chábera, P.; Shao, S.; Zhang, F.; Pullerits, T. Fast Monolayer Adsorption and Slow Energy Transfer in CdSe Quantum Dot Sensitized ZnO Nanowires. *J. Phys. Chem. A* **2013**, *117*, 5919−5925.

DOI: 10.1021/acsomega.7b00316
ACS Omega 2017, 2, 1922−1929